ACS SyntheticBiology

pubs.acs.org/synthbio

Research Article

Expression of Fluorescence Reporters and Natural Products in Native Gut *Escherichia coli*

Dake Liu, Phuong M. Ton, David Zong, Amir Zarrinpar, and Yousong Ding*

Cite This: *ACS Synth. Biol.* 2025, 14, 1557−1566

Read Online

ACCESS | Metrics & More | Article Recommendations | Supporting Information

ABSTRACT: *Escherichia coli* is a widely studied model organism and an integral component of the human gut microbiome, offering significant potential for bacteria-based therapeutic applications. Despite this promise, engineering native *E. coli* strains remains challenging. In this study, we employed the chassis-independent recombinase-assisted genome engineering (CRAGE) technique to genetically engineer the native gut strain *E. coli* EcAZ-1 and the probiotic strain *E. coli* Nissle 1917 (EcN). We successfully expressed a suite of heterologous genes, including the bioluminescent *lux* operon, green fluorescent protein (GFP), and oxygen-independent fluorescent protein IFP2.0, in both strains. Optimization of IFP2.0 fluorescence was achieved under both aerobic and anaerobic conditions by coexpressing a heme oxygenase gene and/or supplementing the chromophore biliverdin or hemin. Additionally, we engineered these strains to biosynthesize the bioactive compounds naringenin and mycosporine-like amino acids. This work highlights the potential of native *E. coli* strains as versatile platforms for synthetic biology, paving the way for innovative applications in biomedical research and therapeutic development.

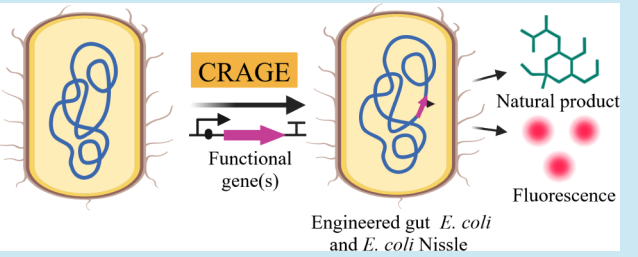

KEYWORDS: *native E. coli, E. coli Nissle 1917, synthetic biology, fluorescent proteins, natural products, hypoxic conditions*

INTRODUCTION

Microbes are ubiquitously present in almost all environmental niches.[1] They play pivotal roles in ecological balance and processes essential for life on Earth, such as nutrient cycling, decomposition, food digestion, immunity, and the biosynthesis of chemicals. With the advent of genetic engineering, the modification of microbial genomes has become a promising strategy for addressing multiple societal challenges,[2] ranging from human health and climate change to sustainability and waste recycling. Despite significant progress, the transformative potential of microbes remains largely underexploited. Recent advances in DNA sequencing technologies have shed light on the extensive genetic diversity of environmental microbes,[3,4] uncovering a realm of untapped microbial functionality. However, the natural microbial repertoire often lacks the specific traits needed for the desired applications. Over the past decades, synthetic biology has demonstrated successes in augmenting the capabilities of microbes, endowing them with enhanced or novel functionalities.[5−8] On the other hand, this progress has so far been predominantly focused on a limited set of domesticated or model microbial strains, which are more tractable to genetic manipulation.[9]

The human gut microbiota, comprising potentially over 1000 species,[10,11] exemplifies the complex interplay between microbes and human health. Alterations in the microbiome have been linked to a broad spectrum of diseases, including cancer, obesity, diabetes, mental health disorders, cardiovascular diseases, inflammatory bowel disease, and infections,[12] as well as influencing the efficacy of therapeutic interventions.[13] Given the notable role of the human microbiome in maintaining and sustaining host health, microbiome engineering emerges as a promising avenue for health improvement and disease mitigation.[14,15] Indeed, the advances of next-generation sequencing and bioinformatics have uncovered the genomes of thousands of microbiome isolates.[16,17] These advances facilitate a deeper understanding of microbiota functionality down to the strain level.[18] Furthermore, new bacterial culturing methods make it possible to isolate >1000 bacterial species from the human gut microbiome,[19,20] and some isolates have been used to construct the synthetic microbial community to investigate the interplays between the microbiome and human health.[21] Nonetheless, the genetic manipulation of microbiome isolates to achieve desired functionalities presents significant challenges,[15,22,23] with only a few strains, such as *Escherichia coli* Nissle 1917 (EcN),[24] *Bifidobacterium*, *Bacteroides*, and lactic acid bacteria,[25,26] being extensively studied.

Received: December 3, 2024
Revised: March 20, 2025
Accepted: March 20, 2025
Published: March 26, 2025

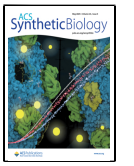

https://doi.org/10.1021/acssynbio.4c00835
ACS Synth. Biol. 2025, 14, 1557−1566

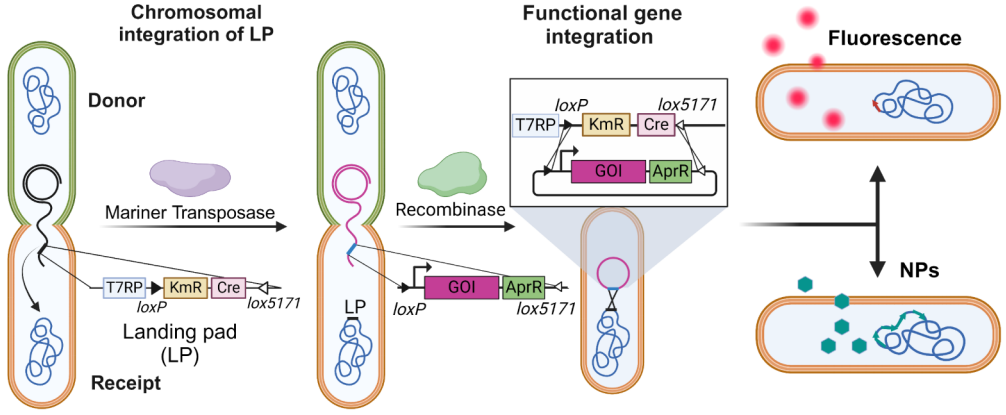

Figure 1. Schematic representation of genetic engineering of EcAZ-1 and ECN by a chassis-independent recombinase-assisted genome engineering (CRAGE) method to express fluorescent proteins and natural products. LP, landing pad; T7RP, T7 RNA polymerase; KmR, kanamycin-resistant gene; AprR, apramycin-resistant gene; Cre, Cre recombinase gene; GOI, gene of interest; NP, natural product.

E. coli is one of the most well-characterized model organisms and has been instrumental in advancing our understanding of genetics, molecular biology, physiology, and biochemistry.[27] Despite its well-characterized status, *E. coli* exhibits significant population diversity[28,29] with an estimated population in nature reaching 10^{20}. This bacterium predominantly resides within the mammalian intestinal microbiome,[30] accounting for 0.1−5% of the total community. However, its pathogenic variants, classified into at least 11 pathotypes, contribute to a spectrum of intestinal and extraintestinal diseases in humans,[31] leading to nearly one million deaths worldwide in 2019.[32] The intricate relationship between *E. coli* and human health is further highlighted by the presence of the genotoxic *pks*+ *E. coli*, which harbors a 50-kb colibactin biosynthetic gene cluster (BGC). These strains are found in approximately 20% of healthy individuals, 40% of patients with inflammatory bowel disease, and 60% of colorectal cancer patients.[33−35] The genetic manipulation of *E. coli* offers a pathway to deepen our understanding of these interactions, yet challenges persist. Wild or undomesticated strains of *E. coli* often resist genetic modification techniques developed for lab-adapted strains,[36] posing a significant barrier to both fundamental and applied microbial research.

Here, we present the genetic engineering of a native *E. coli* strain, EcAZ-1,[37] isolated from the fecal sample of a conventionally raised C57BL/6 male mouse alongside EcN. EcAZ-1 has demonstrated the ability to persistently colonize the gut of conventionally raised mice and express transgenes that can offer protective effects in glucose homeostasis.[38] We successfully employed a transposon-based genomic recombination method to modify both EcAZ-1 and EcN.[39] Using this method, we incorporated an oxygen-independent fluorescent protein, IFP2.0,[40] into their genomes. IFP2.0's fluorescence level was further enhanced by coexpressing a heme oxygenase and supplying the chromophore of IFP2.0 biliverdin (BV) or hemin. Furthermore, we successfully expressed IFP2.0 in both EcAZ-1 and EcN under the control of three hypoxia-specific promoters. Finally, both strains were engineered to produce bioactive natural products (NPs) naringenin and mycosporine-like amino acids,[41] showcasing the potential of genetically engineered native *E. coli* in biomedical research and applications.

RESULTS AND DISCUSSION

EcAZ-1 and EcN Can Be Engineered by CRAGE. Like most gut-derived strains, EcAZ-1 remains undomesticated,[38] and traditional genetic modification methods such as transformation or transduction have largely failed to introduce the genetic material. To address this barrier, we sought to engineer EcAZ-1 using the chassis-independent recombinase-assisted genome engineering (CRAGE) method (Figure 1),[39] which has enabled the chromosomal integration of genetic materials up to 100 kb in size in diverse bacteria. The success of CRAGE in engineering lab *E. coli* BL21 and EPI300[42,43] motivated us to evaluate its application to EcAZ-1. This method starts by introducing an accessory plasmid pW17 into *E. coli* EcAZ-1. The plasmid carries a landing pad (LP) sequence equipped with a *cre* recombinase gene flanked by distinct lox sites and an enhanced Himar1 mariner transposase. The LP also contains a T7 RNA polymerase under the control of an IPTG-inducible promoter, enabling precise gene expression via a T7 promoter. The transposase facilitates the random chromosomal integration of the LP (Figure 1), hereafter referred to as the LP-containing EcAZ-1.[44] Subsequently, the region between the loxP and lox5171 sites is replaced with desired genetic constructs using the Cre recombinase. To our delight, the first pass at conjugation of EcAZ-1 with the conjugation donor *E. coli* WM6026 harboring pW17[39] yielded about 1000 colonies, indicating that EcAZ-1 could be engineered using this method. To further improve the conjugation efficiency, we tested various donor (*E. coli* WM6026 harboring pW17) to recipient (EcAZ-1) ratios (2:1, 4:1, 6:1, and 10:1) and incubation times (12 and 24 h). Optimal conditions were identified as a 6:1 donor-to-recipient ratio and a 12 h incubation, which produced over 3500 conjugants in a single experiment.

We then randomly selected an LP-containing EcAZ-1 colony, confirmed by PCR (Figure S1) as described previously.[39] This colony displayed growth comparable to the wild type (WT) (Figure S2), and we used the optimized conditions to conjugate it with *E. coli* WM6026 containing pW34, a plasmid carrying the *luxCDABE* operon (*lux*).[39] Upon IPTG induction, 57 out of 96 randomly picked colonies produced luminescence (SD = 954.05 units; coefficient of variation = 11.4%) (Figure 2A). Negative control LP-containing EcAZ-1 showed no luminescence signal upon IPTG induction. Additionally, we integrated and expressed the

https://doi.org/10.1021/acssynbio.4c00835
ACS Synth. Biol. 2025, 14, 1557−1566

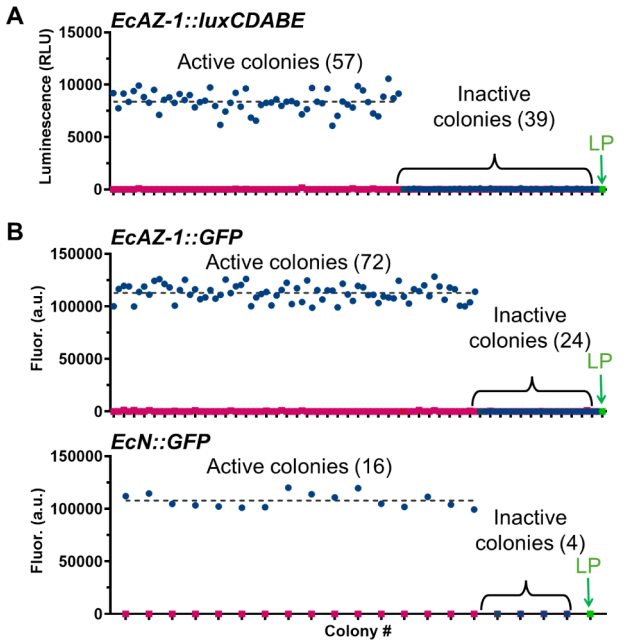

Figure 2. Genetic engineering of EcAZ-1 and EcN via the CRAGE method. **A.** Luminescence analysis of 96 randomly selected colonies of EcAZ-1 engineered to express the *luxCDABE* operon, induced by 0.1 mM IPTG in 96-well microplates. Dark and pink dots represent the signals of induced and uninduced colonies, respectively. LP-containing EcAZ-1 (green dot) served as the negative control. A black-dashed line indicates the average luminescence intensity across all of the positive colonies. RLU: relative light unit. **B.** Fluorescence analysis of randomly picked 96 colonies of EcAZ-1 and 20 colonies of EcN expressing *GFP*. Culture was induced by 0.1 mM IPTG and incubated for 5 h at 37 °C. Fluorescence measurements were taken in 96-well microplates, using an excitation wavelength of 488 nm and an emission wavelength of 510 nm. The data represent the mean ± SD of three independent experiments. a.u.: arbitrary units.

lux operon in EcN using the CRAGE method (Figure S1). All eight randomly picked EcN conjugants produced luminescence after IPTG induction (Figure S3). These results confirm that CRAGE is effective for engineering EcAZ-1 and EcN.

We further validated CRAGE by replacing the *lux* operon in pW34 with the green fluorescent protein (GFP) and repeated the conjugation in both LP-containing EcAZ-1 and EcN. About 75−80% of randomly picked colonies (96 for EcAZ-1 and 20 for EcN) generated fluorescence signals upon IPTG induction, with EcAZ-1 conjugants showing a slightly higher average signal than EcN (mean ± SD: EcAZ-1 = 112,782.4 ± 7852.2 fluorescent units; EcN = 107,772.9 ± 6795.7 fluorescent units) (Figure 2B). Negligible fluorescence was observed in the WT- and LP-containing strains. Overall, our results establish CRAGE as a robust method for the genetic engineering of both undomesticated and probiotic *E. coli* strains.

Expression of the Oxygen-Independent Fluorescent Protein IFP2.0 in EcAZ-1 and EcN. Solid tumors commonly exhibit a hypoxic microenvironment, which significantly impacts cancer progression and treatment outcomes, including increased metastasis risk, therapy resistance, and poor prognosis.[45] Previous efforts have explored the use of bacteria, particularly anaerobes, for targeted delivery to these hypoxic zones within tumors.[46,47] Building on this concept, we aimed to engineer facultative anaerobes EcAZ-1 and EcN to produce a fluorescent signal specifically under hypoxic conditions to enhance tumor imaging capabilities. For this purpose, we selected IFP2.0, an engineered oxygen-independent, bacteriophytochrome-based infrared fluorescent protein, for its superior performance in whole-body imaging of mice compared to traditional oxygen-dependent fluorescent proteins like GFP.[40] Because of these properties, IFP2.0 offers significantly enhanced imaging capabilities in hypoxic environments, despite having a lower fluorescence quantum yield. We replaced the *lux* operon with a codon-optimized *IFP2.0* gene (Table S1) in the plasmid pW34. We then introduced the construct into *E. coli* WM6026 for conjugation with the LP-containing EcAZ-1 and EcN. We randomly selected 20 conjugants of each engineered strain and assessed their fluorescence signals upon IPTG induction under anaerobic conditions. Consistent with the GFP expression results (Figure 2B), more than 75% of the conjugants generated detectable fluorescent signals (Figure S4), which were comparable between engineered EcN and EcAZ-1 (mean ± SD: EcN = 2042.3 ± 328.1 fluorescent units; EcAZ-1 = 2794 ± 109.6 fluorescent units, Figure 3A). Negligible fluorescence was observed in WT or LP-containing strains under anaerobic conditions as well as in positive conjugants without IPTG

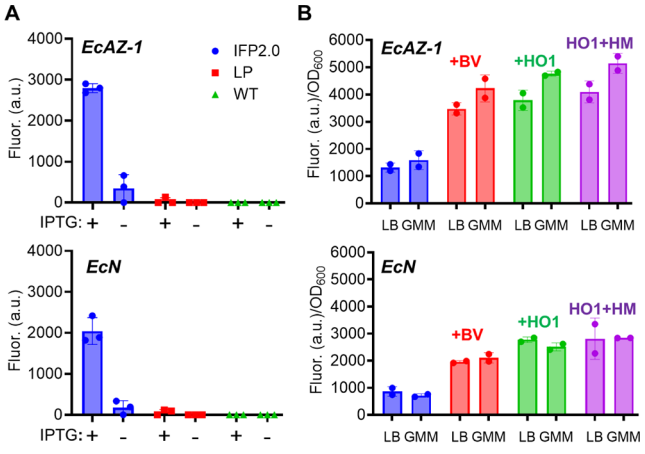

C Ratio of fluorescence signals of engineered EcAZ-1 and EcN in GMM/LB

	IFP2.0	IFP2.0+BV	IFP2.0+HO1	IFP2.0+HO1+HM
EcAZ-1	1.2	1.2	1.3	1.3
EcN	0.8	1.1	0.9	1.0

Figure 3. Expression of oxygen-independent fluorescent protein IFP2.0 in EcAZ-1 and EcN. (A) Fluorescence analysis of engineered EcAZ-1 and EcN expressing IFP2.0. Expressions of IFP2.0 in engineered EcAZ-1 and EcN were induced by 0.1 mM IPTG in LB at 37 °C overnight under anaerobic conditions. Fluorescence measurements were taken in clear-bottom 96-well microplates using an excitation wavelength of 690 nm and an emission wavelength of 710 nm. The average fluorescence intensity of positive colonies is shown. Data represent the mean ± standard deviation of three independent experiments. (B) Improving the fluorescence intensity in EcAZ-1 and EcN by either supplementing BV or coexpressing HO1 in the presence or absence of heme (HM). Expressions of IFP2.0 and HO1 were induced by 0.1 mM IPTG in either GMM or LB at 37 °C overnight under aerobic conditions. The fluorescence was measured in a clear-bottomed 96-well plate. The medium was supplemented with BV (2 μM) or hemin (2 μM). Data are generated after normalization with the growth and presented as the mean ± SD of two independent experiments. (C) Media effects on fluorescence signals. The ratios of fluorescence signals were compared for engineered EcAZ-1 and EcN cultures in LB and GMM.

https://doi.org/10.1021/acssynbio.4c00835
ACS Synth. Biol. 2025, 14, 1557−1566

induction. These results demonstrate the successful expression of IFP2.0 in EcAZ-1 and EcN, which could potentially be applied to enhanced imaging of hypoxic regions within tumors.

However, we found that GFP exhibited a fluorescence signal at least 40 times stronger than that of IFP2.0 in engineered EcAZ-1 and EcN (Figures 2 and 3), highlighting potential areas for improvement. Since biliverdin (BV) is the chromophore of IFP2.0,[40] we hypothesized that limited BV availability could be restricting IFP2.0's fluorescence intensity in these strains. To test this, we selected one positive colony exhibiting an average fluorescent signal (Figure S4) and then induced its IFP2.0 expression by IPTG in both Luria−Bertani (LB) and gut microbiota medium (GMM), supplemented with 2 μM BV. After normalizing cell growth, this supplementation enhanced the fluorescence levels of engineered EcAZ-1 and EcN by 2.6 times in both media after overnight incubation (Figure 3B), suggesting that enhancing BV availability could improve the IFP2.0 fluorescence intensity. Notably, fluorescence intensities of engineered EcAZ-1 were higher in GMM than in LB, whereas LB supported slightly higher fluorescence levels for engineered EcN (Figure 3B,C). To further augment BV cellular availability, we introduced a codon-optimized heme oxygenase gene (HO1) from *Bradyrhizobium* sp. (Table S1),[48] along with *IFP2.0*, replacing the *lux* operon in the plasmid pW34.[39] HO1 enzymatically converts hemin to BV in the presence of O_2, thereby potentially increasing the intracellular pool of IFP2.0's chromophore. The two genes were integrated into the same locus of the chromosome of LP carrying EcAZ-1 and EcN. We screened ten randomly picked conjugants and selected one representative clone from each strain (EcAZ-1-IFP2.0+HO1 or EcN-IFP2.0+HO1) with average fluorescence levels for further analysis. After normalizing for cell growth, the coexpression of HO1 enhanced the fluorescence intensity of EcAZ-1-IFP2.0 by about threefold in both LB and GMM (Figure 3B), with similar improvements observed for EcN-IFP2.0+HO1. Supplementation with 2 μM hemin, the substrate of HO1, further boosted the signal in EcAZ-1-IFP2.0+HO1 by 1.1 times on average, demonstrating the slight synergistic effect of precursor supplementation and coexpression of HO1 in boosting fluorescence output. Interestingly, hemin supplementation resulted in only a slight increase in the fluorescence intensity for EcN-IFP2.0+HO1 in GMM, with no improvement in LB (Figure 3B). Overall, compared with LB, GMM supported higher fluorescence signals in EcAZ-1 but not in EcN (Figure 3C). These results collectively indicate that the coexpression of IFP2.0 and HO1, combined with hemin or BV supplementation, significantly enhances the fluorescence level of engineered bacterial strains.

Expression of IFP2.0 in EcAZ-1 and EcN under Hypoxia Conditions. Noninvasive tumor imaging in vivo using engineered bacteria demands hypoxia-specific inducible systems. We thus evaluated IFP2.0 expression in LB under the control of three FNR (fumarate and nitrate reduction)-dependent hypoxia-inducible promoters, including Pfnr,[49] FF20, and FF20*, alongside the T7 promoter as a positive control in anaerobic conditions. The Pfnr promoter series, particularly the engineered variants FF20 and FF20*, exhibits high oxygen sensitivity in *E. coli* and other organisms, demonstrating equal or superior strength compared to other hypoxia-specific promoters (e.g., PPepT and PVgb) for regulating protein expression in *E. coli*.[50] Notably, FF20* retained 77−84% of its activity under pathological hypoxia in vivo (0.1−0.5% O_2) but was reduced to minimal levels under mild hypoxic or normoxic conditions.[51] We cloned IFP2.0 under the control of these promoters into the backbone of pW34 and integrated the cassette into the chromosome of LP carrying EcAZ-1 and EcN. Similarly, over 75% of randomly selected colonies displayed fluorescence signals, and one positive colony with an average intensity was selected for each promoter for further analysis. In EcAZ-1, IFP2.0 expression under the T7 promoter was 1.5- to 1.9-fold higher compared to the tested hypoxia-specific promoters (Figure 4A). To assess promoter dynamics in EcAZ-1, we measured

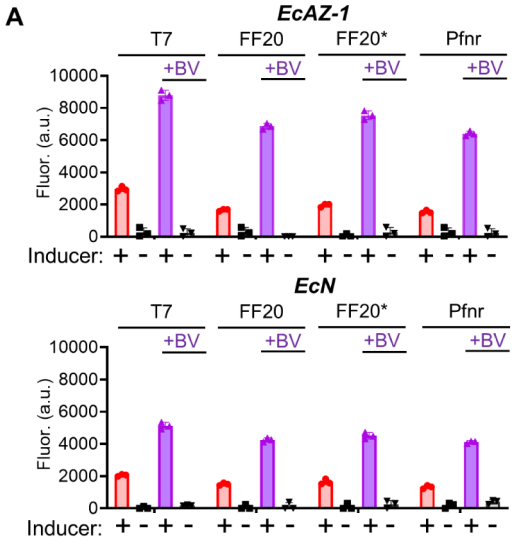

B

Fold of signal improvement by BV supplementation

	T7	FF20	FF20*	Pfnr
EcAZ-1	3.0	4.1	3.9	4.2
EcN	2.5	2.8	2.7	3.1

Figure 4. Hypoxia promoters activate the expression of IFP2.0 in EcAZ-1 and EcN under anaerobic conditions. (A) Fluorescence analysis of EcAZ-1 and EcN expressing *IFP2.0* controlled by T7, Pfnr, FF20, and FF20* promoters. Engineered strains were cultured in LB in 96-well microplates at 37 °C until the log phase. The protein expression was then induced by 0.1 mM IPTG for the T7 promoter or was placed under anaerobic conditions for the hypoxia promoters. BV (2 μM) was supplied, and the cultures were further incubated overnight. Fluorescence measurements were taken in clear-bottom 96-well microplates using an excitation wavelength of 690 nm and an emission wavelength of 710 nm. Aerobic fermentation was used as the negative condition for hypoxia-specific promoters. The data represent the mean ± standard deviation of three independent experiments. (B) Effect of BV supplementation on fluorescent signals. The fold improvement of fluorescence intensity by BV supplementation was calculated by dividing the fluorescence intensity of a sample supplemented with BV from that without BV supplementation.

fluorescence at 0, 1, 3, 5, and 20 h (Figure S5). After 1 h, the fluorescence of IFP2.0 under T7 promoter control reached around 22.4% of its maximal fluorescence intensity, while those controlled by Pfnr, FF20, and FF20* promoters reached about 17.6%, 14.2%, and 14.3%, respectively. During the first 5 h, the fluorescence increase rate for the T7 system was 1902.8 units/h, compared to 1316.2 units/h for Pfnr, 1388.6 units/h for FF20, and 1516.4 units/h for FF20*. Under aerobic conditions, fluorescence from the hypoxia-specific promoters did not increase over time (Figure S5). Similarly, FF20, FF20*, and Pfnr drove significant expression of IFP2.0 in EcN under

https://doi.org/10.1021/acssynbio.4c00835
ACS Synth. Biol. 2025, 14, 1557−1566

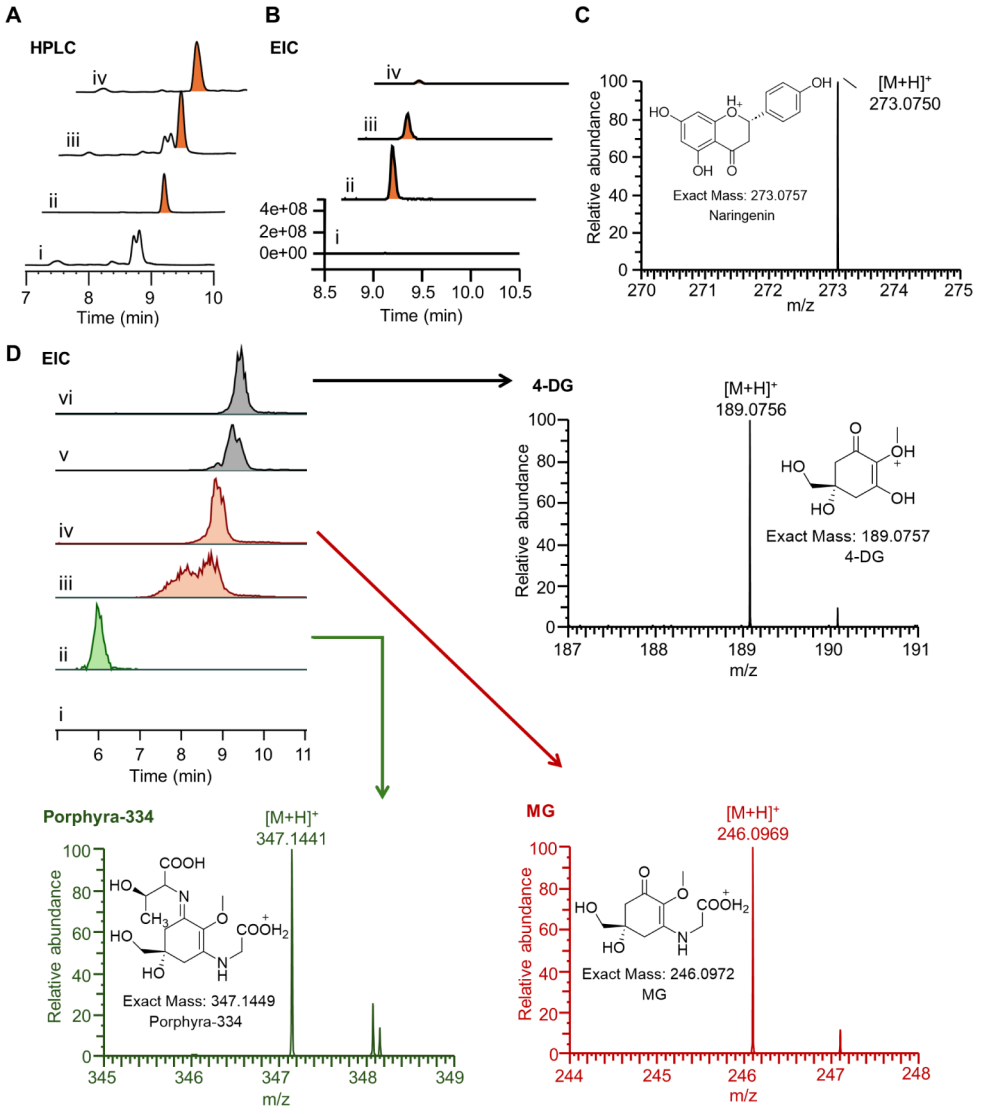

Figure 5. Heterologous production of bioactive naringenin and mycosporine-like amino acids in EcAZ-1 and EcN. (A) HPLC analysis of EcAZ-1 expressing the naringenin BGC under aerobic (iii) and anaerobic (ii) conditions. Engineered EcAZ-1 without IPTG induction under aerobic conditions (i) and naringenin standard (iv) served as controls. The detection wavelength is 283 nm. (B) Extracted ion chromatogram (EIC, m/z = 273.03−273.13) shows traces of ethyl acetate extraction of engineered EcAZ-1 (iii) and EcN (iv). Engineered EcAZ-1 without IPTG induction (i) and naringenin standard (ii) served as controls. The experiments were conducted under aerobic conditions. (C) HRMS analysis of naringenin produced by engineered EcAZ-1. (D) EIC traces of porphyra-334 (m/z = 347.1439−347.1459, ii), MG (m/z = 246.0965−246.0979, iv), and 4-DG (m/z = 189.0751−189.0763, iv) in the methanolic extraction of EcAZ-1 engineered with the MAA BGC. Standard MG (ii) and 4-DG (iv) served as controls, and engineered EcAZ-1 without IPTG induction acted as a negative control. The induced production of MAAs was performed under aerobic conditions. HRMS traces of 4-DG, MG, and porphyra-334 produced by engineered EcAZ-1 showed expected m/z values. EIC and MS traces of different metabolite molecules are shown with different colors.

anaerobic conditions (Figure S6), although the expression was lower compared to EcAZ-1 (Figure 4A). Supplementation of 2 μM BV further enhanced IFP2.0 fluorescence regulated by hypoxia-specific promoters in both EcAZ-1 and EcN by 2.7 to 4.2 times (Figure 4), reaching fluorescence levels comparable to those under T7 promoter control. Similar results were observed when these experiments were performed in GMM (Figure S7), where both engineered strains showed slightly improved growth compared with LB (Figure S8). After growth normalization, engineered EcAZ-1 and EcN produced comparable fluorescence signals (fluorescence/OD_{600}) in both media (Figure S7). Furthermore, BV supplementation resulted in a greater improvement of fluorescence signals controlled by hypoxia-dependent promoters in both strains in LB, compared with the T7 promoter (Figure 4B). A similar improvement across all promoters was observed in GMM (Figure S7C). Collectively, these results underscore the effectiveness of hypoxia-specific promoters in regulating IFP2.0 expression under anaerobic conditions, demonstrating the potential of engineered EcAZ-1 and EcN as cancer-specific imaging tools.

Heterologous Production of Naringenin and Mycosporine-Like Amino Acids in EcAZ-1 and EcN. Natural products have long been used for human health maintenance and disease treatment.[52,53] *E. coli* is a model synthetic biology chassis in the heterologous production of natural products.[54] We sought to evaluate if the native gut *E. coli* EcAZ-1 can be used to produce bioactive natural products. We first tested the

https://doi.org/10.1021/acssynbio.4c00835
ACS Synth. Biol. 2025, 14, 1557−1566

production of the flavone naringenin, which is produced by a variety of plants and shows many beneficial effects on human health, such as scavenging reactive oxidative species and modulating carbohydrate metabolism and immune responses.[55] Starting from L-tyrosine, the biosynthesis of naringenin requires four enzymes: L-tyrosine ammonia-lyase (TAL), 4-coumarate-CoA ligase (4CL), chalcone synthase (CHS), and chalcone isomerase (CHI) (Figure S9A). We synthesized these four genes, assembled as a single operon under the control of the T7 promoter (Table S1), and cloned the pathway into vector pW5Y for conjugation with LP-containing EcAZ-1. We randomly picked one colony confirmed by PCR for producing naringenin (Figure S10). After IPTG induction and overnight incubation at 18 (aerobic) or 37 °C (anaerobic) and shaking at 180 rpm, the bacterial cultures were extracted three times with equal volumes of ethyl acetate. The combined organic layers were dried and resuspended in 200 μL of acetonitrile for analysis by HPLC and LC-MS. We observed the production of naringenin under both aerobic and anaerobic conditions (Figure 5A), with aerobic production being approximately 1.3 times higher. This difference may be attributed to the increased temperature during anaerobic fermentation. The identity of naringenin was confirmed by HRMS-EIC analysis (observed $[M + H]^+$ = 273.0750, calculated $[M + H]^+$ = 273.0757) (Figure 5C) and HR-MS/MS fragmentation (Figure S11A), matching the authentic standard. Similarly, we engineered EcN to express the naringenin BGC and observed the production of naringenin under aerobic conditions (Figure 5B). The aerobic yield of naringenin in EcAZ-1 was determined as 202 ng/mL that is about 9 times higher than EcN (23 ng/mL), which might be relevant to the differences in their genetic background and chromosomal location of the inserted BGC.[56,57]

We further evaluated the capability of EcAZ-1 to produce mycosporine-like amino acids (MAAs), a family of natural UV protectants.[58] MAAs also possess anti-inflammatory, antioxidative, and antiaging properties. The biosynthesis of disubstituted MAAs starts from the conversion of an intermediate of the pentose phosphate pathway, sedoheptulose 7-phosphate, into 4-deoxygadusol (4-DG) by MysA (a dehydroquinate synthase homologue) and MysB (an *O*-methyltransferase) (Figure S9B).[58] Subsequently, MysC and MysD, two ATP-grasp enzymes, sequentially produce mycosporine-glycine (MG) and disubstituted MAA analogs such as porphyra-334. Using the same method as the heterologous production of naringenin in EcAZ-1 and EcN, we expressed the MAA BGC from the cyanobacterium *Nostoc linckia* NIES-25[59] under the control of the T7 promoter. After induction by 0.1 mM IPTG at 18 °C and 200 rpm overnight under aerobic conditions, HPLC, HRMS, and HRMS/MS analysis revealed the production of porphyra-334 (observed $[M + H]^+$ = 347.1441, calculated $[M + H]^+$ = 347.1449) as well as biosynthetic intermediates MG (observed $[M + H]^+$ = 246.0969, calculated $[M + H]^+$ = 246.0972) and 4-DG (observed $[M + H]^+$ = 189.0756, calculated $[M + H]^+$ = 189.0757) by the engineered EcAZ-1 (Figures 5D and S11B–D). We observed a lower yield of these compounds under anaerobic conditions (Figure S12), which might be due to the altered metabolic flux and slower growth of EcAZ-1.[60,61] We performed the same experiments for the integration and expression of the MAA BGC in EcN. MG and porphyra-334 were produced by EcN under both aerobic and anaerobic conditions (Figure S12). No 4-DG was detected in the anaerobic fermentation of engineered EcAZ-1 and EcN. Altogether, our results demonstrated that EcAZ-1 and EcN are promising chassis to produce different families of bioactive molecules, presenting new opportunities to develop bacteria-based approaches to sustain human health.

In conclusion, our work demonstrates the efficacy of the CRAGE method in genetically engineering native and probiotic *E. coli* strains EcAZ-1 and EcN, respectively. The successful integration of functional genes such as *GFP* and *IFP2.0* into these strains not only underscores the versatility of CRAGE but also enhances our capabilities for detailed functional studies and biotechnological applications in health and disease contexts. Notably, the engineered strains exhibited fluorescence signals under both aerobic and anaerobic conditions, demonstrating their potential as imaging tools for studying hypoxic tumor microenvironments in the future. Additionally, the successful production of bioactive natural products in engineered EcAZ-1 emphasizes the expanded biotechnological applications of this strain, which robustly colonizes the gut of conventionally raised mice.[38] Naringenin is known for its immunomodulatory and anticancer properties,[55] while MAAs are recognized for their antioxidant and anti-inflammatory activities.[58] This study also encourages the further exploration of native microbiota as a rich resource for addressing complex biological challenges.[62] The CRAGE method employs a transposon-based system combined with conjugation (Figure 1) to introduce single or multiple genes into a broad range of nonmodel species, including members of Proteobacteria and Actinobacteria.[39] While EcN has traditionally been engineered with only one or a few genes, primarily through transformation,[24,50] this study expanded its genetic toolkit by utilizing the conjugation-based CRAGE method for the highly efficient integration of large genetic constructs. More recently, the CRAGE method has been improved with the integration of clustered regularly interspaced short palindromic repeats (CRISPR) technology, enabling precise genome editing of recipient cells[63] and further broadening its potential for engineering undomesticated *E. coli* strains. Future work would also aim to leverage the CRAGE method to manipulate genetically resistant, undomesticated strains widely available in diverse environments and rigorously assess the functionalities of engineered EcAZ-1 and EcN in cellular and animal models. These efforts hold considerable promise for advancing microbiome-based therapeutic strategies and synthetic biology innovations.

MATERIALS AND METHODS

General Methods. Reagents and chemicals were purchased from major vendors, e.g., Thermo Scientific, New England Biolabs, Fisher Scientific, and Sigma-Aldrich. Plasmid preparation and DNA purification were performed with a GeneJET Plasmid Miniprep Kit and a GeneJET Gel Extraction Kit (Thermo Scientific), respectively. Genes were synthesized by Twist Bioscience. Primers were ordered from Sigma-Aldrich. *E. coli* DH5α (Agilent) was used for routine cloning. *E. coli* Nissle 1917 (EcN) was provided by Ardeypharm, Germany. The plasmids pW17, pW5Y, and pW34 were obtained from Addgene with catalog IDs 158207, 158211, and 158210, respectively.

Engineering of EcAZ-1 and EcN by the CRAGE Method. We followed the published experimental procedures of the CRAGE method.[39] To optimize the conjugation

https://doi.org/10.1021/acssynbio.4c00835
ACS Synth. Biol. 2025, 14, 1557−1566

efficiency between EcAZ-1 and *E. coli* WM6026, we mixed different ratios of the donor (*E. coli* WM6026 harboring pW17) to the recipient (EcAZ-1) (2:1, 4:1, 6:1, and 10:1) and washed the mixture three times with fresh LB. The pellets were then resuspended in 50 μL LB with 0.3 mM DAP (diaminopimelic acid) and transferred onto a nitrocellulose filter membrane on an LB agar plate containing 0.3 mM DAP. The plate was then incubated at 37 °C for 12 or 24 h. The bacterial mixtures were then scraped off and washed with 1 mL of fresh LB three times. The pellets were then resuspended in 1 mL of fresh LB, and 100 μL of the mixtures were plated on an LB plate containing 50 μg/mL kanamycin. Following overnight incubation at 37 °C, the numbers of grown colonies were counted to evaluate the conjugation efficiencies under different conjugation conditions. The chromosomal integration of the landing pad from pW17 in the recipient was then confirmed by PCR analysis of about 3−7 randomly picked colonies (Figure S1, Table S2).

Fluorescence Protein Expression and Fluorescence Measurement. To construct the fluorescent protein-expressing strains, the backbone of pW34 (without the luxABCD operon) was ligated with synthetic *IFP2.0*, *IFP2.0+HO1*, or *GFP* genes at *Bam*HI/*Eco*RI sites, along with the T7, Pfnr, FF20, or FF20* promoter. Subsequent conjugation and chromosomal integration into LP-containing EcAZ-1/EcN followed the CRAGE method.[39] The gene integration was verified by colony PCR and antibiotic counterselection. Fluorescent protein-expressing strains were grown in 2 mL of medium (LB or gut microbiota medium, GMM) containing 50 μg/mL apramycin at 37 °C and shaking at 250 rpm overnight. The cultures were then diluted 1000 times into 96-well clear-bottom microplates, each well containing 200 μL of LB or GMM with 50 μg/mL apramycin. After growing at 37 °C and 220 rpm until the log phase, the protein expression was induced by 0.1 mM IPTG or by anaerobic conditions in an anaerobic chamber (Whitley DG250 Anaerobic Workstation). BV (2 μM) or heme (2 μM) may also be supplied to the culture medium at this time. Culture tubes or 96-well plates were covered with aluminum foil to protect BV from light. For anaerobic experiments, all necessary materials, reagents, and media were degassed and preincubated in the chamber in advance. After induction, strains were then incubated at 37 °C and 220 rpm for 12−20 h aerobically or anaerobically. Before fluorescence measurements, 96-well microplates containing anaerobic cultures were sealed with a parafilm. Fluorescence measurements of the samples were carried out on a BioTek Synergy H1 Multimode Reader with excitation at 690 nm and emission at 710 nm for IFP2.0 expression and with excitation at 488 nm and emission at 510 nm for GFP expression. The fluorescence from wild-type strains or those integrated with the LP as negative controls was used for the normalization of fluorescence signals. Two to three technical replicates were conducted for the measurement. The OD_{600} values of the samples were also measured.

Heterologous Production of Naringenin and MAA. To construct the naringenin BGC, synthesized genes encoding TAL, 4CL, CHS, and CHI were inserted into the *Xho*I, *Hind*III, *Sac*I, and *Bam*HI, respectively, on pET28b (+) along with the T7 promoter (Table S1). The gene cluster was then amplified and cloned into the *Not*I/*Sac*II sites of pW5Y to create pW5Y-Nar. To construct the MAA BGC, the *mysABCD* cluster along with the T7 promoter was amplified from pETDuet-1-*mysABCD*[59] and cloned into *Not*I/*Sac*II sites of pW5Y to create pW5Y-MAA. The conjugation and chromosomal integration into EcAZ-1 and EcN followed the CRAGE method and the procedure described above. To evaluate the production of naringenin or MAA, engineered strains were cultured in 100 or 200 mL of LB containing 50 μg/mL apramycin at 37 °C and 220 rpm until the OD_{600} reached 0.6. Protein expression was then induced by adding 0.1 mM IPTG and culturing at 18 or 37 °C at 180 rpm overnight. Anaerobic fermentation was performed in an anaerobic chamber (Whitley DG250 Anaerobic Workstation). All necessary materials, reagents, and media for anaerobic experiments were degassed and incubated in the chamber overnight in advance. Strains were inoculated and grown in the chamber at 37 °C overnight prior to the experiments. BGC expressions, culture incubations, strain harvesting, and liquid−liquid extractions were conducted in the chamber. The extracted collections in glass vials were sealed with parafilm and immediately subjected to evaporation using a rotary evaporator. The other conditions were the same as aerobic experiments. To prepare naringenin extracts, the culture was extracted with an equal volume of ethyl acetate three times. The organic extracts were collected, combined, dried, and evaporated in the speed vacuum concentrator. The residues were resuspended in 200 μL acetonitrile, and after centrifugation, 10 μL of the solution was injected for HPLC and HRLC-MS for analysis. To extract MAAs, cell pellets were collected after centrifugation at 4500 rpm for 10 min and then extracted with 2 mL of methanol twice. Methanolic extracts were combined and dried in the speed vacuum concentrator, and the residues were resuspended in 200 μL water for LC-HRMS and HR-MS/MS for analysis.

HPLC and LC-MS Analysis. HPLC analysis was performed on a Shimadzu Prominence UHPLC system (Kyoto, Japan) fitted with an Agilent Poroshell 120 EC-C18 column (2.7 μm, 4.6 mm × 50 mm), coupled with a PDA detector. The HPLC program started with 1% solvent B (methanol with 0.1% formic acid) for 1 min, followed by a linear gradient of 1−20% solvent B in 3 min and another linear gradient of 20−95% solvent B in 4 min. The column was further cleaned with 95% solvent B for 1 min and then re-equilibrated with 1% solvent B for 1 min. Solvent A was water with 0.1% formic acid. The flow rate was set at 0.5 mL/min. The same LC program was used in the LC-MS analysis on a Thermo Scientific TSQ Altis Plus Triple Quadrupole Mass Spectrometer with a Thermo Scientific Vanquish HPLC system. The system was equipped with an H-ESI ion source. Molecules in samples were analyzed in both negative and positive modes at 3500 and 2500 V, respectively. Electrospray ionization was used for MS detection, and ion counts for a particular m/z peak were determined by peak height. LC-HRMS and HRMS/MS were conducted on a Thermo Scientific Q Exactive Focus mass spectrometer with a Dionex Ultimate RSLC 3000 uHPLC system, equipped with the H-ESI II probe on an Ion Max API Source. Acetonitrile (B)/water (A) containing 0.1% formic acid was used as the mobile phase. The LC analysis was performed using the same program parameters as those used for the HPLC analysis. The eluents from the first 1 min were diverted to waste by a diverting valve. The gradient is such that that B phase increases from 5% to 95% from 2 to 12 min, keeps 95% for 1 min, and then drops back 5% in 1 min. MS1 signals were acquired under the full MS positive ion mode, covering a mass range of m/z 150−750, with the resolution at 35,000 and AGC target at 1×10^6. Fragmentation was obtained with

https://doi.org/10.1021/acssynbio.4c00835
ACS Synth. Biol. 2025, 14, 1557−1566

parallel reaction monitoring (PRM) using an inclusion list of calculated parental ions. The AGC target was set at 5×10^4 for MS2. Precursor ions were selected in the quadrupole, typically with an isolation width of 3.0 m/z, and fragmented in the HCD cell at a collision energy (CE) of 20.

■ ASSOCIATED CONTENT

Supporting Information

The Supporting Information is available free of charge at https://pubs.acs.org/doi/10.1021/acssynbio.4c00835.

Synthetic gene sequences and primers; additional data about the characterization of engineered EcAZ-1 and EcN in growth and fluorescent signal generation, biosynthesis of natural products, and MS/MS fragmentation (PDF)

■ AUTHOR INFORMATION

Corresponding Author

Yousong Ding − *Department of Medicinal Chemistry, Center for Natural Products, Drug Discovery and Development, University of Florida, Gainesville, Florida 32610, United States;* orcid.org/0000-0001-8610-0659; Email: yding@cop.ufl.edu

Authors

Dake Liu − *Department of Medicinal Chemistry, Center for Natural Products, Drug Discovery and Development, University of Florida, Gainesville, Florida 32610, United States*

Phuong M. Ton − *Department of Medicinal Chemistry, Center for Natural Products, Drug Discovery and Development, University of Florida, Gainesville, Florida 32610, United States*

David Zong − *Division of Gastroenterology, University of California, San Diego, La Jolla, California 92093, United States*

Amir Zarrinpar − *Division of Gastroenterology, University of California, San Diego, La Jolla, California 92093, United States; Shu Chien-Gene Lay Department of Bioengineering and Center for Microbiome Innovation, University of California San Diego, La Jolla, California 92093, United States; Division of Gastroenterology, Jennifer Moreno Department of Veterans Affairs Medical Center, La Jolla, California 92093, United States*

Complete contact information is available at: https://pubs.acs.org/10.1021/acssynbio.4c00835

Author Contributions

Y.D., A.Z., and D.L. conceived and designed the project. D.L. and P.T. performed experiments and collected data. D.L. and Y.D. contributed to the data analysis. D.L., D.Z., A.Z., and Y.D. wrote and edited the manuscript. All authors approved the submitted manuscript.

Notes

The authors declare the following competing financial interest(s): A.Z. is a co-founder and acting CMO of Endure Biotherapeutics. He holds equity in the company.

■ ACKNOWLEDGMENTS

We are grateful to Prof. William W. Metcalf at the University of Illinois at Urbana−Champaign for providing *E. coli* WM6026 and Drs. Manyun Chen and Dipesh Dhakal from the Ding Group for providing the biosynthetic gene clusters. We also thank Ms. Yujia Jiang for her technical support. This work is supported by the National Institutes of Health U01 CA265719 (to Y.D. and A.Z.). A.Z. is supported by NIH R01 EB030134, R01 AI163483, and VA Merit BLR&D Award I01 BX005707. He also receives institutional support from NIH P30 DK120515, P30 DK063491, and UL1 TR001442.

■ REFERENCES

(1) Falkowski, P. G.; Fenchel, T.; Delong, E. F. The microbial engines that drive Earth's biogeochemical cycles. *Science* **2008**, *320*, 1034−1039.

(2) Can microbes save the planet?. In *Nat. Biotechnol.*, **2023**; Vol. *41*, pp. 735−735. DOI: .

(3) Sunagawa, S.; Coelho, L. P.; Chaffron, S.; Kultima, J. R.; Labadie, K.; Salazar, G.; Djahanschiri, B.; Zeller, G.; Mende, D. R.; Alberti, A.; et al. Ocean plankton. Structure and function of the global ocean microbiome. *Science* **2015**, *348*, 1261359.

(4) Bardgett, R. D.; van der Putten, W. H. Belowground biodiversity and ecosystem functioning. *Nature* **2014**, *515*, 505−511.

(5) Khalil, A. S.; Collins, J. J. Synthetic biology: applications come of age. *Nat. Rev. Genet.* **2010**, *11*, 367−379.

(6) Keasling, J. D. Synthetic biology for synthetic chemistry. *ACS Chem. Biol.* **2008**, *3*, 64−76.

(7) McCarty, N. S.; Ledesma-Amaro, R. Synthetic biology tools to engineer microbial communities for biotechnology. *Trends Biotechnol.* **2019**, *37*, 181−197.

(8) Hillson, N.; Caddick, M.; Cai, Y.; Carrasco, J. A.; Chang, M. W.; Curach, N. C.; Bell, D. J.; Le Feuvre, R.; Friedman, D. C.; Fu, X.; Gold, N. D.; Herrgard, M. J.; Holowko, M. B.; Johnson, J. R.; Johnson, R. A.; Keasling, J. D.; Kitney, R. I.; Kondo, A.; Liu, C.; Martin, V. J. J.; Menolascina, F.; Ogino, C.; Patron, N. J.; Pavan, M.; Poh, C. L.; Pretorius, I. S.; Rosser, S. J.; Scrutton, N. S.; Storch, M.; Tekotte, H.; Travnik, E.; Vickers, C. E.; Yew, W. S.; Yuan, Y.; Zhao, H.; Freemont, P. S. Building a global alliance of biofoundries. *Nat. Commun.* **2019**, *10*, 2040.

(9) Adams, B. L. The next generation of synthetic biology chassis: Moving synthetic biology from the laboratory to the field. *ACS Synth. Biol.* **2016**, *5*, 1328−1330.

(10) Sender, R.; Fuchs, S.; Milo, R. Revised estimates for the number of human and bacteria cells in the body. *PloS Biol.* **2016**, *14*, No. e1002533.

(11) Yan, Q.; Li, S.; Yan, Q.; Huo, X.; Wang, C.; Wang, X.; Sun, Y.; Zhao, W.; Yu, Z.; Zhang, Y.; Guo, R.; Lv, Q.; He, X.; Yao, C.; Li, Z.; Chen, F.; Ji, Q.; Zhang, A.; Jin, H.; Wang, G.; Feng, X.; Feng, L.; Wu, F.; Ning, J.; Deng, S.; An, Y.; Guo, D. A.; Martin, F. M.; Ma, X. A genomic compendium of cultivated human gut fungi characterizes the gut mycobiome and its relevance to common diseases. *Cell.* **2024**, *187* (12), 2969−2989.e24.

(12) Ogunrinola, G. A.; Oyewale, J. O.; Oshamika, O. O.; Olasehinde, G. I. The Human microbiome and its impacts on health. *Int. J. Microbiol.* **2020**, *2020*, 8045646.

(13) Hou, K.; Wu, Z.-X.; Chen, X.-Y.; Wang, J.-Q.; Zhang, D.; Xiao, C.; Zhu, D.; Koya, J. B.; Wei, L.; Li, J.; Chen, Z.-S. Microbiota in health and diseases. *Signal Transduct. Target. Ther.* **2022**, *7* (1), 135.

(14) Jin, W.-B.; Li, T.-T.; Huo, D.; Qu, S.; Li, X. V.; Arifuzzaman, M.; Lima, S. F.; Shi, H.-Q.; Wang, A.; Putzel, G. G.; Longman, R. S.; Artis, D.; Guo, C.-J. Genetic manipulation of gut microbes enables single-gene interrogation in a complex microbiome. *Cell.* **2022**, *185*, 547−562 e522.

(15) Bai, X.; Huang, Z.; Duraj-Thatte, A. M.; Ebert, M. P.; Zhang, F.; Burgermeister, E.; Liu, X.; Scott, B. M.; Li, G.; Zuo, T. Engineering the gut microbiome. *Nat. Rev. Bioeng.* **2023**, *1*, 665−679.

(16) Forster, S. C.; Kumar, N.; Anonye, B. O.; Almeida, A.; Viciani, E.; Stares, M. D.; Dunn, M.; Mkandawire, T. T.; Zhu, A.; Shao, Y.; Pike, L. J.; Louie, T.; Browne, H. P.; Mitchell, A. L.; Neville, B. A.; Finn, R. D.; Lawley, T. D. A human gut bacterial genome and culture

collection for improved metagenomic analyses. *Nat. Biotechnol.* **2019**, *37*, 186−192.
(17) Almeida, A.; Nayfach, S.; Boland, M.; Strozzi, F.; Beracochea, M.; Shi, Z. J.; Pollard, K. S.; Sakharova, E.; Parks, D. H.; Hugenholtz, P.; Segata, N.; Kyrpides, N. C.; Finn, R. D. A unified catalog of 204,938 reference genomes from the human gut microbiome. *Nat. Biotechnol.* **2021**, *3939*, 105−114.
(18) Patnode, M. L.; Guruge, J. L.; Castillo, J. J.; Couture, G. A.; Lombard, V.; Terrapon, N.; Henrissat, B.; Lebrilla, C. B.; Gordon, J. I. Strain-level functional variation in the human gut microbiota based on bacterial binding to artificial food particles. *Cell Host Microbe* **2021**, *29*, 664−673.e665.
(19) Browne, H. P.; Forster, S. C.; Anonye, B. O.; Kumar, N.; Neville, B. A.; Stares, M. D.; Goulding, D.; Lawley, T. D. Culturing of'unculturable' human microbiota reveals novel taxa and extensive sporulation. *Nature* **2016**, *533*, 543−546.
(20) Lagier, J.-C.; Khelaifia, S.; Alou, M. T.; Ndongo, S.; Dione, N.; Hugon, P.; Caputo, A.; Cadoret, F.; Traore, S. I.; Seck, E. H.; Dubourg, G.; Durand, G.; Mourembou, G.; Guilhot, E.; Togo, A.; Bellali, S.; Bachar, D.; Cassir, N.; Bittar, F.; Delerce, J.; Mailhe, M.; Ricaboni, D.; Bilen, M.; Dangui Nieko, N. P. M.; Dia Badiane, N. M.; Valles, C.; Mouelhi, D.; Diop, K.; Million, M.; Musso, D.; Abrahao, J.; Azhar, E. I.; Bibi, F.; Yasir, M.; Diallo, A.; Sokhna, C.; Djossou, F.; Vitton, V.; Robert, C.; Rolain, J. M.; La Scola, B.; Fournier, P. E.; Levasseur, A.; Raoult, D. RETRACTED ARTICLE: Culture of previously uncultured members of the human gut microbiota by culturomics. *Nat. Microbiol.* **2016**, *1* (12), 16203.
(21) Cheng, A. G.; Ho, P.-Y.; Aranda-Diaz, A.; Jain, S.; Yu, F. B.; Meng, X.; Wang, M.; Iakiviak, M.; Nagashima, K.; Zhao, A.; Murugkar, P.; Patil, A.; Atabakhsh, K.; Weakley, A.; Yan, J.; Brumbaugh, A. R.; Higginbottom, S.; Dimas, A.; Shiver, A. L.; Deutschbauer, A.; Neff, N.; Sonnenburg, J. L.; Huang, K. C.; Fischbach, M. A. Design, construction, and in vivo augmentation of a complex gut microbiome. *Cell* **2022**, *185*, 3617−3636 e3619.
(22) Cubillos-Ruiz, A.; Guo, T.; Sokolovska, A.; Miller, P. F.; Collins, J. J.; Lu, T. K.; Lora, J. M. Engineering living therapeutics with synthetic biology. *Nat. Rev. Drug Discovery* **2021**, *20*, 941−960.
(23) Kelly, V. W.; Liang, B. K.; Sirk, S. J. Living therapeutics: The next frontier of precision medicine. *ACS Synth. Biol.* **2020**, *9*, 3184−3201.
(24) Lynch, J. P.; Goers, L.; Lesser, C. F. Emerging strategies for engineering *Escherichia coli* Nissle 1917-based therapeutics. *Trends Pharmacol. Sci.* **2022**, *43*, 772−786.
(25) Bermudez-Humaran, L. G.; Aubry, C.; Motta, J. P.; Deraison, C.; Steidler, L.; Vergnolle, N.; Chatel, J. M.; Langella, P. Engineering *Lactococci* and *Lactobacilli* for human health. *Curr. Opin. Microbiol.* **2013**, *16*, 278−283.
(26) Zuo, F.; Chen, S.; Marcotte, H. Engineer probiotic *Bifidobacteria* for food and biomedical applications - Current status and future prospective. *Biotechnol. Adv.* **2020**, *45*, 107654.
(27) Hobman, J. L.; Penn, C. W.; Pallen, M. J. Laboratory strains of *Escherichia coli*: Model citizens or deceitful delinquents growing old disgracefully? *Mol. Microbiol.* **2007**, *64*, 881−885.
(28) Whitman, W. B.; Coleman, D. C.; Wiebe, W. J. Prokaryotes: the unseen majority. *Proc. Natl. Acad. Sci. U. S. A.* **1998**, *95*, 6578−6583.
(29) Denamur, E.; Clermont, O.; Bonacorsi, S.; Gordon, D. The population genetics of pathogenic *Escherichia coli*. *Nat. Rev. Microbiol.* **2021**, *19*, 37−54.
(30) Tenaillon, O.; Skurnik, D.; Picard, B.; Denamur, E. The population genetics of commensal *Escherichia coli*. *Nat. Rev. Microbiol.* **2010**, *8*, 207−217.
(31) Geurtsen, J.; de Been, M.; Weerdenburg, E.; Zomer, A.; McNally, A.; Poolman, J. Genomics and pathotypes of the many faces of *Escherichia coli*. *FEMS Microbiol. Rev.* **2022**, *46* (6), fuac031.
(32) GBD 2019 Antimicrobial Resistance Collaborators. Global mortality associated with 33 bacterial pathogens in 2019: a systematic analysis for the Global Burden of Disease Study 2019. *Lancet* **2022**, *400*, 2221−2248.
(33) Nougayrede, J. P.; Homburg, S.; Taieb, F.; Boury, M.; Brzuszkiewicz, E.; Gottschalk, G.; Buchrieser, C.; Hacker, J.; Dobrindt, U.; Oswald, E. *Escherichia coli* induces DNA double-strand breaks in eukaryotic cells. *Science* **2006**, *313*, 848−851.
(34) Dejea, C. M.; Fathi, P.; Craig, J. M.; Boleij, A.; Taddese, R.; Geis, A. L.; Wu, X.; DeStefano Shields, C. E.; Hechenbleikner, E. M.; Huso, D. L.; Anders, R. A.; Giardiello, F. M.; Wick, E. C.; Wang, H.; Wu, S.; Pardoll, D. M.; Housseau, F.; Sears, C. L. Patients with familial adenomatous polyposis harbor colonic biofilms containing tumorigenic bacteria. *Science* **2018**, *359*, 592−597.
(35) Arthur, J. C.; Perez-Chanona, E.; Muhlbauer, M.; Tomkovich, S.; Uronis, J. M.; Fan, T. J.; Campbell, B. J.; Abujamel, T.; Dogan, B.; Rogers, A. B.; Rhodes, J. M.; Stintzi, A.; Simpson, K. W.; Hansen, J. J.; Keku, T. O.; Fodor, A. A.; Jobin, C. Intestinal inflammation targets cancer-inducing activity of the microbiota. *Science* **2012**, *338*, 120−123.
(36) Liu, D.; Siguenza, N. E.; Zarrinpar, A.; Ding, Y. Methods of DNA introduction for the engineering of commensal microbes. *Eng. Microbiol.* **2022**, *2*, 100048.
(37) Siguenza, N.; Russell, B. J.; Richter, R. A.; Zarrinpar, A. Complete genome sequence of an *Escherichia coli* strain isolated from laboratory mouse stool for use as a chassis for transgene delivery to the murine microbiome. *Microbiol. Res. Announc.* **2023**, *12*, No. e0101422.
(38) Russell, B. J.; Brown, S. D.; Siguenza, N.; Mai, I.; Saran, A. R.; Lingaraju, A.; Maissy, E. S.; Machado, A. C. D.; Pinto, A. F. M.; Sanchez, C.; Rossitto, L. A.; Miyamoto, Y.; Richter, R. A.; Ho, S. B.; Eckmann, L.; Hasty, J.; Gonzalez, D. J.; Saghatelian, A.; Knight, R.; Zarrinpar, A. Intestinal transgene delivery with native *E. coli* chassis allows persistent physiological changes. *Cell* **2022**, *185*, 3263−3277 e3215.
(39) Wang, G.; Zhao, Z.; Ke, J.; Engel, Y.; Shi, Y. M.; Robinson, D.; Bingol, K.; Zhang, Z.; Bowen, B.; Louie, K.; Wang, B.; Evans, R.; Miyamoto, Y.; Cheng, K.; Kosina, S.; De Raad, M.; Silva, L.; Luhrs, A.; Lubbe, A.; Hoyt, D. W.; Francavilla, C.; Otani, H.; Deutsch, S.; Washton, N. M.; Rubin, E. M.; Mouncey, N. J.; Visel, A.; Northen, T.; Cheng, J. F.; Bode, H. B.; Yoshikuni, Y. CRAGE enables rapid activation of biosynthetic gene clusters in undomesticated bacteria. *Nat. Microbiol.* **2019**, *4*, 2498−2510.
(40) Yu, D.; Gustafson, W. C.; Han, C.; Lafaye, C.; Noirclerc-Savoye, M.; Ge, W. P.; Thayer, D. A.; Huang, H.; Kornberg, T. B.; Royant, A.; Jan, L. Y.; Jan, Y. N.; Weiss, W. A.; Shu, X. An improved monomeric infrared fluorescent protein for neuronal and tumour brain imaging. *Nat. Commun.* **2014**, *5*, 3626.
(41) Punchakara, A.; Prajapat, G.; Bairwa, H. K.; Jain, S.; Agrawal, A. Applications of mycosporine-like amino acids beyond photoprotection. *Appl. Environ. Microbiol.* **2023**, *89*, No. e0074023.
(42) Ke, J.; Zhao, Z.; Coates, C. R.; Hadjithomas, M.; Kuftin, A.; Louie, K.; Weller, D.; Thomashow, L.; Mouncey, N. J.; Northen, T. R.; Yoshikuni, Y. Development of platforms for functional characterization and production of phenazines using a multi-chassis approach via CRAGE. *Metab. Eng.* **2022**, *69*, 188−197.
(43) Noonan, A. J. C.; Qiu, Y.; Ho, J. C. H.; Ocampo, J.; Vreugdenhil, K. A.; Marr, R. A.; Zhao, Z.; Yoshikuni, Y.; Hallam, S. J. CRAGE-mediated insertion of fluorescent chromosomal markers for accurate and scalable measurement of co-culture dynamics in *Escherichia coli*. *Synth. Biol.* **2020**, *5*, ysaa015.
(44) Lampe, D. J.; Akerley, B. J.; Rubin, E. J.; Mekalanos, J. J.; Robertson, H. M. Hyperactive transposase mutants of the Himar1 mariner transposon. *Proc. Natl. Acad. Sci. U. S. A.* **1999**, *96*, 11428−11433.
(45) Jing, X.; Yang, F.; Shao, C.; Wei, K.; Xie, M.; Shen, H.; Shu, Y. Role of hypoxia in cancer therapy by regulating the tumor microenvironment. *Mol. Cancer* **2019**, *18* (1), 157.
(46) Xiao, S.; Shi, H.; Zhang, Y.; Fan, Y.; Wang, L.; Xiang, L.; Liu, Y.; Zhao, L.; Fu, S. Bacteria-driven hypoxia targeting delivery of chemotherapeutic drug proving outcome of breast cancer. *J. Nanobiotechnol.* **2022**, *20*, 178.

https://doi.org/10.1021/acssynbio.4c00835
ACS Synth. Biol. 2025, 14, 1557−1566

(47) Luo, C. H.; Huang, C. T.; Su, C. H.; Yeh, C. S. Bacteria-mediated hypoxia-specific delivery of nanoparticles for tumors imaging and therapy. *Nano Lett.* **2016**, *16*, 3493−3499.
(48) Giraud, E.; Hannibal, L.; Fardoux, J.; Vermeglio, A.; Dreyfus, B. Effect of *Bradyrhizobium* photosynthesis on stem nodulation of *Aeschynomene sensitiva*. *Proc. Natl. Acad. Sci. U. S. A.* **2000**, *97*, 14795−14800.
(49) Spiro, S.; Roberts, R. E.; Guest, J. R. FNR-dependent repression of the *ndh* gene of *Escherichia coli* and metal ion requirement for FNR-regulated gene expression. *Mol. Microbiol.* **1989**, *3*, 601−608.
(50) Chien, T.; Harimoto, T.; Kepecs, B.; Gray, K.; Coker, C.; Hou, N.; Pu, K.; Azad, T.; Nolasco, A.; Pavlicova, M.; Danino, T. Enhancing the tropism of bacteria via genetically programmed biosensors. *Nat. Biomed. Eng.* **2022**, *6*, 94−104.
(51) Ryan, R. M.; Green, J.; Williams, P. J.; Tazzyman, S.; Hunt, S.; Harmey, J. H.; Kehoe, S. C.; Lewis, C. E. Bacterial delivery of a novel cytolysin to hypoxic areas of solid tumors. *Gene Ther.* **2009**, *16*, 329−339.
(52) Dias, D. A.; Urban, S.; Roessner, U. A historical overview of natural products in drug discovery. *Metabolites* **2012**, *2*, 303−336.
(53) Atanasov, A. G.; Zotchev, S. B.; Dirsch, V. M.; Supuran, C. T.; International Natural Product Sciences. Natural products in drug discovery: advances and opportunities. *Nat. Rev. Drug Discovery* **2021**, *20* (3), 200−216.
(54) Ahmadi, M. K.; Pfeifer, B. A. Recent progress in therapeutic natural product biosynthesis using *Escherichia coli*. *Curr. Opin. Biotechnol.* **2016**, *42*, 7−12.
(55) Ucar, K.; Goktas, Z. Biological activities of naringenin: A narrative review based on *in vitro* and *in vivo* studies. *Nutr. Res.* **2023**, *119*, 43−55.
(56) Bryant, J. A.; Sellars, L. E.; Busby, S. J.; Lee, D. J. Chromosome position effects on gene expression in *Escherichia coli* K-12. *Nucleic Acids Res.* **2014**, *42*, 11383−11392.
(57) Hong, C. K. Y.; Ramu, A.; Zhao, S.; Cohen, B. A. Effect of genomic and cellular environments on gene expression noise. *Genome Biol.* **2024**, *25* (1), 137.
(58) Chen, M.; Jiang, Y.; Ding, Y. Recent progress in unraveling the biosynthesis of natural sunscreens mycosporine-like amino acids. *J. Ind. Microbiol. Biotechnol.* **2023**, *50* (1), kuad038.
(59) Chen, M.; Rubin, G. M.; Jiang, G.; Raad, Z.; Ding, Y. Biosynthesis and heterologous production of mycosporine-like amino acid palythines. *J. Org. Chem.* **2021**, *86*, 11160−11168.
(60) Wang, Q.; Ou, M. S.; Kim, Y.; Ingram, L. O.; Shanmugam, K. T. Metabolic flux control at the pyruvate node in an anaerobic *Escherichia coli* strain with an active pyruvate dehydrogenase. *Appl. Environ. Microbiol.* **2010**, *76*, 2107−2114.
(61) Gonzalez, J. E.; Long, C. P.; Antoniewicz, M. R. Comprehensive analysis of glucose and xylose metabolism in *Escherichia coli* under aerobic and anaerobic conditions by ^{13}C metabolic flux analysis. *Metab. Eng.* **2017**, *3939*, 9−18.
(62) Marsh, J. W.; Kirk, C.; Ley, R. E. Toward microbiome engineering: Expanding the repertoire of genetically tractable members of the human gut microbiome. *Annu. Rev. Microbiol.* **2023**, *77*, 427−449.
(63) Ke, J.; Robinson, D.; Wu, Z. Y.; Kuftin, A.; Louie, K.; Kosina, S.; Northen, T.; Cheng, J. F.; Yoshikuni, Y. CRAGE-CRISPR facilitates rapid activation of secondary metabolite biosynthetic gene clusters in bacteria. *Cell Chem. Biol.* **2022**, *29*, 696−710.

https://doi.org/10.1021/acssynbio.4c00835
ACS Synth. Biol. 2025, 14, 1557−1566